nature COMMUNICATIONS

ARTICLE

Received 4 Sep 2014 | Accepted 2 Feb 2015 | Published 12 Mar 2015

DOI: 10.1038/ncomms7485

Surface transfer doping induced effective modulation on ambipolar characteristics of few-layer black phosphorus

Du Xiang[1,2,*], Cheng Han[1,2,*], Jing Wu[1,2,3,*], Shu Zhong[4], Yiyang Liu[2,4], Jiadan Lin[1,2], Xue-Ao Zhang[5], Wen Ping Hu[6,7], Barbaros Özyilmaz[1,2,3], A.H. Castro Neto[1,2], Andrew Thye Shen Wee[1,2] & Wei Chen[1,2,4,8]

Black phosphorus, a fast emerging two-dimensional material, has been configured as field effect transistors, showing a hole-transport-dominated ambipolar characteristic. Here we report an effective modulation on ambipolar characteristics of few-layer black phosphorus transistors through *in situ* surface functionalization with caesium carbonate (Cs_2CO_3) and molybdenum trioxide (MoO_3), respectively. Cs_2CO_3 is found to strongly electron dope black phosphorus. The electron mobility of black phosphorus is significantly enhanced to $\sim 27\ cm^2\ V^{-1}\ s^{-1}$ after 10 nm Cs_2CO_3 modification, indicating a greatly improved electron-transport behaviour. In contrast, MoO_3 decoration demonstrates a giant hole-doping effect. *In situ* photoelectron spectroscopy characterization reveals significant surface charge transfer occurring at the dopants/black phosphorus interfaces. Moreover, the surface-doped black phosphorus devices exhibit a largely enhanced photodetection behaviour. Our findings coupled with the tunable nature of the surface transfer doping scheme ensure black phosphorus as a promising candidate for further complementary logic electronics.

[1] Department of Physics, National University of Singapore, Singapore 117542, Singapore. [2] Centre for Advanced 2D Materials and Graphene Research Centre, National University of Singapore, 6 Science Drive 2, Singapore 117546, Singapore. [3] NanoCore, National University of Singapore, Singapore 117576, Singapore. [4] Department of Chemistry, National University of Singapore, 3 Science Drive 3, Singapore 117543, Singapore. [5] College of Science, National University of Defense Technology, Changsha 410073, China. [6] Beijing National Laboratory for Molecular Sciences, Key Laboratory of Organic Solids, Institute of Chemistry, Chinese Academy of Sciences, Beijing 100190, China. [7] Department of Chemistry, School of Science, Tianjin University and Collaborative Innovation Center of Chemical Science and Engineering (Tianjin), Tianjin 300072, China. [8] National University of Singapore (Suzhou) Research Institute, 377 Lin Quan Street, Suzhou Industrial Park, Jiang Su 215123, China. * These authors contributed equally to this work. Correspondence and requests for materials should be addressed to W.C. (email: phycw@nus.edu.sg).

Two-dimensional (2D) layered materials such as graphene and transition metal dichalcogenides (TMDs) have been considered as promising building blocks for the next-generation nanoelectronic devices, showing great potentials to extend the scaling limits existing in silicon-based complementary metal oxide semiconductor field effect transistors (CMOS-FET)[1–3], as well as to serve as a high-mobility alternative to organic semiconductors for flexible electronic and optoelectronic devices[4,5]. Graphene, as the forefather of 2D materials[6], has exhibited extremely high carrier mobility ($>100{,}000\ cm^2\ V^{-1}\ s^{-1}$; ref. 7) and a wealth of fundamental physical properties[8–10]. However, graphene-based electronic devices seriously suffer from the absence of an intrinsic bandgap, which strongly limits the application of graphene in logic electronics[11]. Recently, TMDs with an inherent bandgap have emerged as promising materials for both electronic and optoelectronic applications[12–14]. Among the TMD family, molybdenum disulfide (MoS_2) FET devices mostly present the n-type semiconducting behaviour attributed to the intrinsic atomic defects of MoS_2, such as sulfur vacancies, as well as the pronounced Fermi level pinning effect at metal contacts/MoS_2 interface[15,16], which severely restricts its applications in both CMOS transistors and p–n diodes[17,18]. Tungsten diselenide (WSe_2), another member in 2D TMDs, demonstrates the great possibility to be fabricated as complementary logic devices on a single flake resulting from its ambipolar transport characteristics[19–21]. Nevertheless, the device performance of WSe_2 FETs strongly depends on the metal contacts, showing limited carrier mobility without sufficient contact doping[13,22]. Therefore, to further develop atomically thin 2D semiconductors based CMOS electronics, the newly discovered p-type or ambipolar 2D materials with high carrier mobility are highly desirable.

Black phosphorus (BP), a fast emerging 2D material, was recently isolated from the layered BP crystals, where each phosphorus atom is covalently bonded to three neighbouring atoms to form the puckered orthorhombic structure[23,24]. BP has a direct bandgap for all number of layers, predicted from 0.3 eV for bulk to 2 eV for monolayer[25–28]. This characteristic leads to remarkable applications for BP-based optoelectronic devices[24,29]. Moreover, the intrinsic small bandgap allows the few-layer BP to be easily modulated between ON and OFF conduction states. The multilayer BP-configured FET devices demonstrate the clear ambipolar transport behaviour with remarkably high hole mobility up to $\sim 1{,}000\ cm^2\ V^{-1}\ s^{-1}$ and on/off ratio of $\sim 10^5$ at room temperature[23,30], making this material suitable for transistors. On the other hand, the ambipolar characteristics of BP FETs show the strong asymmetry between electron and hole transport[31], where both the concentration and mobility of electrons are orders of magnitude lower than that of holes, making it difficult to fulfil the complementary logic devices on a single BP flake. In order to better control and further enhance the performance of BP-based complementary devices, it is of great significance to effectively tune the n- or p-type doping level of BP.

Chemical doping, as a simple and effective doping approach, has been widely utilized to manipulate the electronic properties of 2D materials as well as organic semiconductors[13,32–36]. Compared with the electrostatic modulation via an external electrical field, chemical doping usually provides a stronger non-volatile doping capability with the ease of device fabrication[37]. Surface transfer doping relies on the interfacial charge transfer without introducing significant defects into the lattice structure of the as-doped materials, thereby nearly reserving their fundamental transport properties[38]. Various organic and inorganic species have demonstrated excellent doping effects on 2D materials such as graphene and TMDs, among which caesium carbonate (Cs_2CO_3) and molybdenum trioxide (MoO_3) have been used to effectively modify the doping level of MoS_2 and grapheme, respectively[32,33]. Furthermore, the contact doping on TMDs FETs, such as MoS_2 and WSe_2, has been shown to remarkably enhance the device performance owing to the effective modulation of Schottky barrier formed at contact/semiconductor interface[13,36].

In the following, we report the surface transfer electron and hole doping to effectively tune the ambipolar characteristics of few-layer BP FETs via *in situ* surface functionalization with Cs_2CO_3 and MoO_3. The BP device is found to be strongly n-type doped by Cs_2CO_3 layer. The electron mobility of BP is significantly increased to $\sim 27\ cm^2\ V^{-1}\ s^{-1}$ after 10 nm Cs_2CO_3 decoration, which leads to highly improved electron transport in BP devices. On the other hand, MoO_3 shows a marked p-type doping effect on BP devices with non-degraded hole mobility. *In situ* ultraviolet photoelectron spectroscopy (UPS) and X-ray photoelectron spectroscopy (XPS) characterization confirm the interfacial charge transfer between BP and doping layers. This doping can also modulate the Schottky junctions formed between metal contacts and BP flakes, and hence to enhance the photoresponsivity of BP-based photodetectors.

Results

Characterization of BP FET devices. Figure 1a displays the atomic force microscopy image of an as-made BP FET device on highly p-doped silicon substrate with 300 nm SiO_2. The line profile reveals the BP flake thickness of $\sim$4.8 nm, that is, $\sim$8 atomic layers. As illustrated in Fig. 1b, the first-order Raman spectrum of exfoliated few-layers BP exhibits the characteristic peaks nearly located at 364, 438 and 465 cm^{-1}, corresponding to the three different vibration modes A^1_g, B_{2g} and A^2_g in BP crystal lattice, respectively[39].

Figure 1c exhibits the typical source-drain current versus source-drain voltage (I_{sd}–V_{sd}) characteristics of the fabricated BP FETs under different gate voltages measured under high vacuum (10^{-8} mbar). Excellent linearity with V_{sd} ranging from -100 to 100 mV suggests the good contact between the metal electrodes and the BP flake. The transfer characteristic (I_{sd}–V_g) of the same device is shown in Fig. 1d. Applying the gate voltage ranging from -70 to 70 V, the source-drain current under 100 mV bias increased along both negative and positive sweeping directions, corresponding to the hole and electron transport, respectively. This indicates a typical ambipolar transport behaviour. Moreover, a much faster current increase was observed in the negative gate voltage region compared with that of the positive side, revealing a hole-transport-dominated ambipolar characteristic. The inset logarithmic plot shows the I_{on}/I_{off} ratio of this BP-based FET to be $\sim 10^4$, which is in good agreement with the previously reported values[23,30]. The threshold voltage V_{th} of the ambipolar device was determined to be approximately -37 V for holes and $\sim$16 V for electrons, extracted from the linear extrapolation of current onset in the linear region of hole and electron side, respectively (Fig. 1e,f). Based on the transfer plot, the carrier concentration induced by gate voltage V_g in the linear region was estimated by the formula below:

$$n = -\frac{C_i(V_g - V_{th})}{e} \quad (1)$$

where C_i is the capacitance per unit area between BP and back gate given by $C_i = \varepsilon_0\varepsilon_r/d$, and ε_r, d are the dielectric constant and thickness of SiO_2, respectively. For example, the hole concentration at $V_g = -50$ V was derived to be 9.3×10^{11} cm^{-2}; while the electron concentration can be estimated to be 1.0×10^{12} cm^{-2} under $V_g = 40$ V. Similarly, the field effect

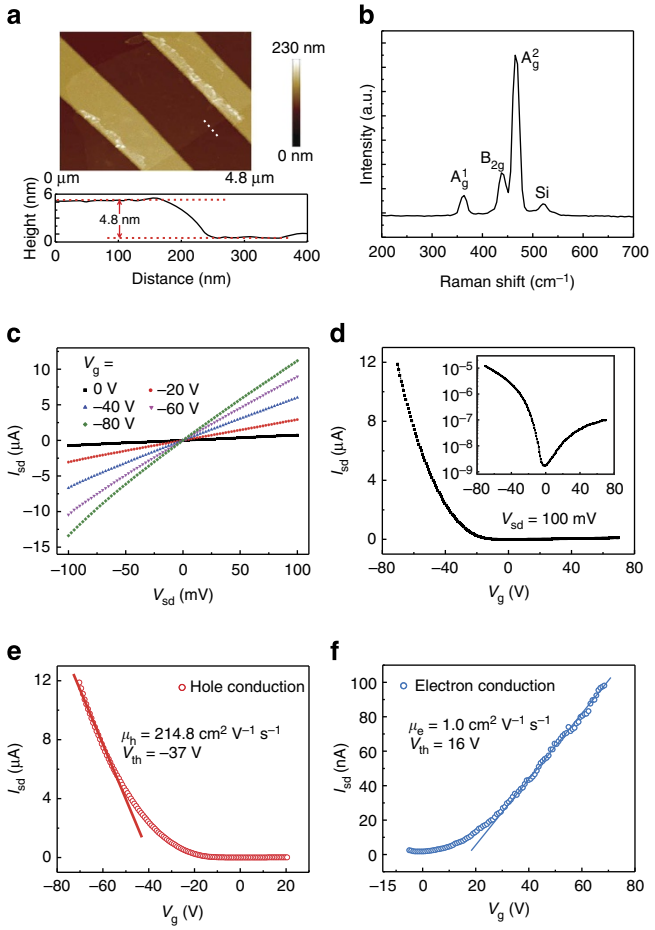

Figure 1 | Few-layer back-gated BP field effect transistor and device characterization. (**a**) Atomic force microscopy image of an as-fabricated BP device. The line profile at the edge of the BP flake indicates a multilayer BP crystal of ~4.8 nm (~8 layers). (**b**) RAMAN spectroscopy of BP flake used for device fabrication. (**c**) I_{sd}–V_{sd} characteristics of a BP FET as a function of different gate voltages from 0 to −80 V. (**d**) Transfer characteristics (I_{sd}–V_g) of the same device with V_{sd} = 100 mV. Inset: logarithmic plot of the transfer curve. Separate transfer curves for (**e**) hole and (**f**) electron conduction, respectively; μ_h and μ_e are the hole and electron mobility respectively; V_{th} is the threshold voltage.

carrier mobility of BP flake can be evaluated via the equation:

$$\mu = \frac{L}{WC_i V_{sd}} \frac{dI_{sd}}{dV_g} \quad (2)$$

where dI_{sd}/dV_g represents the maximum slope extracted from the linear region of transfer characteristic, L and W are the length and width of conduction channel, respectively. For the device illustrated in Fig. 1d, the hole and electron mobility were calculated to be 214.8 and 1.0 cm^2 V^{-1} s^{-1}, respectively.

Surface transfer electron doping on BP devices by Cs_2CO_3. Cs_2CO_3, as an efficient electron-donating material, has been extensively utilized in organic electronics owing to its low work function[40,41]. In order to explore the surface functionalization of Cs_2CO_3 on tuning the electrical transport properties of BP, Cs_2CO_3 was *in situ* evaporated onto the fabricated devices in high vacuum. Figure 2a demonstrates the typical forward transfer characteristics evolution (V_g from −80 to 80 V) in logarithmic scale of BP devices with increasing Cs_2CO_3 thickness. The initial transfer curve without Cs_2CO_3 presents a current minimum of approximately −19 V. As the thickness of Cs_2CO_3 increased to 1.5 nm, the current minimum progressively moved to ~ −64 V. This suggests a significant n-type doping effect on Cs_2CO_3-decorated BP, originating from the interfacial electron transfer from Cs_2CO_3 to BP owing to the large work function difference between them. The backward gate sweeping (V_g from 80 to −80 V) was also implemented on the same Cs_2CO_3-doped BP device (Supplementary Fig. 1). The transfer curve presents the similar negative shifting with increasing Cs_2CO_3 thickness. This indicates that such strong n-type doping effect of Cs_2CO_3 on BP applies to both forward and backward gate sweeping in spite of large hysteresis in BP FETs, as discussed in Supplementary Note 1. The transfer curves coated by 0.5 and 10 nm Cs_2CO_3 were plotted with respect to pristine BP in linear scale as shown in Fig. 2b. At 0.5 nm Cs_2CO_3 coverage, the on-current in electron regime almost reached the same level as that of the hole regime, demonstrating a more symmetric and balanced ambipolar characteristic. With even higher Cs_2CO_3 coverage, the current of electron side gradually evolved beyond the hole side, which indicates an electron-transport-dominated ambipolar behaviour. After 10 nm Cs_2CO_3 deposition, pure n-type transport characteristic was reached in the limited gate voltage range for the modified BP device. The calculated electron concentration (V_g = 30 V) and mobility were plotted as a function of Cs_2CO_3 thickness in Fig. 3a. The estimated electron concentration of BP at 30 V V_g clearly increased from 5.0×10^{11} to 1.5×10^{12} cm^{-2} with the gradual deposition of Cs_2CO_3. More intriguingly, the Cs_2CO_3-functionalized BP device presents almost 25 times enhancement of electron mobility from 1.1 cm^2 V^{-1} s^{-1} for pristine BP to 27.1 cm^2 V^{-1} s^{-1} at 10 nm Cs_2CO_3 coverage, revealing a remarkably improved electron transport in the BP channel. We propose that the undoped BP possesses high concentration of charge (electron) trapping sites, and hence the low electron mobility of undoped BP is mainly limited by the trapped charge scattering. The n-type doping can largely increase electron concentration to fill these trapping sites as well as to effectively screen the trapped charges, and hence the electron mobility can greatly increase as shown in Fig. 3a. Alternatively, the electron doping in BP can also reduce the effective Schottky barrier height between BP and metal contacts, which makes the electron transport in BP not limited by contacts and approach to its intrinsic transport behaviours. In order to figure out the contact resistance between metal electrodes and doped BP channel, four-terminal measurements were also performed on Cs_2CO_3-modified BP devices. As illustrated in Supplementary Fig. 2, the transfer characteristics measured by four-terminal configuration did not show much difference from two-terminal configuration for all Cs_2CO_3 thickness, resulting from the much lower contact resistance compared with the channel resistance (Supplementary Table 1). Moreover, the extracted contact resistance largely decreased with increasing Cs_2CO_3 thickness as predicted, which will be discussed in the last part. This reveals that the contacts between metal and BP channel do not clearly restrict the BP FET performance, and thus the performance enhancement of Cs_2CO_3-decorated BP devices (for example, electron mobility enhancement) mainly originates from the improved intrinsic transport properties of BP channel, not reduced contact resistance (Supplementary Note 2). Owing to the remarkably enhanced electron mobility and concentration, the conductivity of BP was largely increased from 0.01 to 1.37 μS by two orders of magnitudes after 10 nm Cs_2CO_3 deposition, as presented in Fig. 3b. Although the undoped multilayer BP FETs could operate in either hole or electron-transport regime, both the source-drain current and mobility in the electron side are much lower than that of the hole side at equal back gate doping levels.

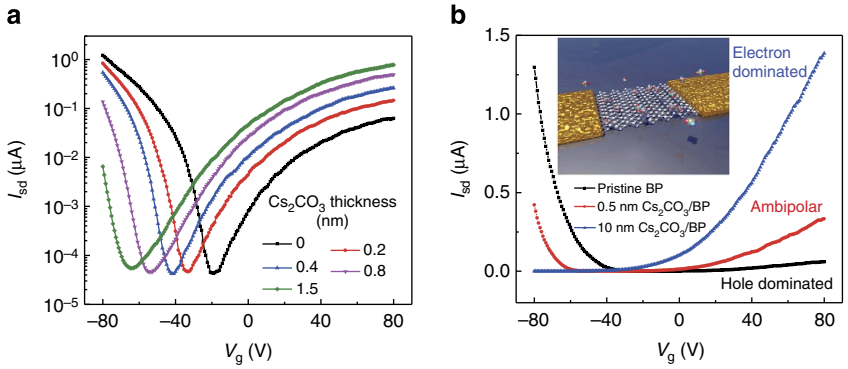

Figure 2 | Transfer characteristics evolution for Cs_2CO_3-modified BP field effect transistor. (**a**) Forward transfer characteristics (V_g from −80 to 80 V) evolution of a BP FET measured at V_{sd} = 100 mV in logarithmic scale with increasing Cs_2CO_3 thickness from 0 to 1.5 nm. (**b**) Linear plot of the transfer curves at 0.5 and 10 nm Cs_2CO_3 coverage with respect to the pristine BP. The electron transport of BP FET was significantly improved after Cs_2CO_3 modification, leading to either a more balanced ambipolar or even electron-transport-dominated FET characteristic. Inset: schematic illustration of BP device coated by Cs_2CO_3.

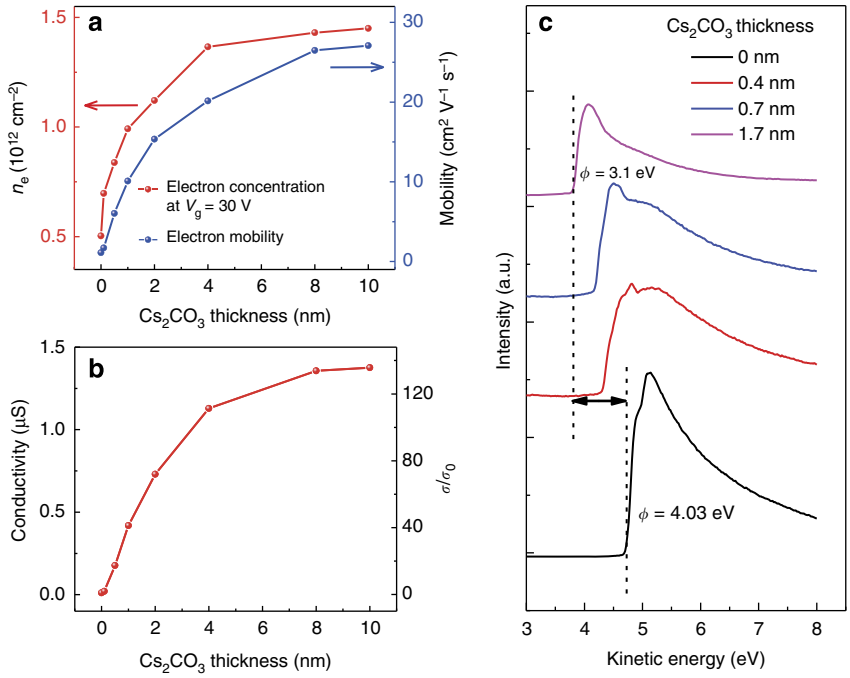

Figure 3 | Analysis of electrical transport properties and UPS evolution for Cs_2CO_3-coated BP. (**a**) Electron concentration (n_e) at V_g = 30 V and mobility of BP versus Cs_2CO_3 thickness. The electron mobility is remarkably enhanced by ~25 times to ~27 cm^2 V^{-1} s^{-1}. (**b**) The plot of BP conductivity (σ) at zero gate voltage as a function of electron concentration. σ_0 is the conductivity of pristine BP. (**c**) UPS spectra evolution at the low kinetic energy region (secondary electron cutoff) with respect to the Cs_2CO_3 thickness. Φ is the work function.

Our results demonstrate that Cs_2CO_3 overlayers can serve as an efficient n-type surface dopant to effectively improve the electron transport in BP devices, thereby inducing either a more balanced ambipolar or even electron-transport-dominated FET behaviour.

In situ UPS/XPS measurements were carried out on Cs_2CO_3-coated bulk BP to further understand the interfacial interaction between Cs_2CO_3 and BP. The evolution of the UPS spectra at the low kinetic energy region with respect to Cs_2CO_3 thickness is exhibited in Fig. 3c. By linearly extrapolating the low kinetic energy onset in UPS spectra, the work function of natural bulk BP was measured to be 4.03 eV. After 1.7 nm Cs_2CO_3 deposition, the work function sharply decreased to 3.1 eV, originating from the substantial interfacial electron transfer from Cs_2CO_3 to BP. This significant charge transfer was also confirmed by the XPS core level spectra of P $2p_{3/2}$, as shown in Supplementary Fig. 3. With increasing Cs_2CO_3 thickness, the P $2p_{3/2}$ peak gradually shifted to higher binding energy region. This indicates a downward band bending of ~0.2 eV coated by 1.7 nm Cs_2CO_3, originating from the increase of electron concentration in Cs_2CO_3-doped BP, and therefore the Fermi level of BP moving closer to the conduction band edge.

Surface transfer hole doping on BP devices by MoO_3. In contrast to the electron doping via Cs_2CO_3, thermally grown MoO_3 layers in high vacuum possess the extremely high work function of ~6.8 eV (ref. 42), and thereby create giant hole-doping effect on few-layer BP FETs. As presented in Fig. 4a, the pristine BP FET exhibits the current minimum located at ~21 V. When the MoO_3 thickness increased to 0.1 nm, the current minimum positively shifted to ~67 V, indicating a marked p-type doping effect of MoO_3 on BP device. Moreover, the transfer curve kept

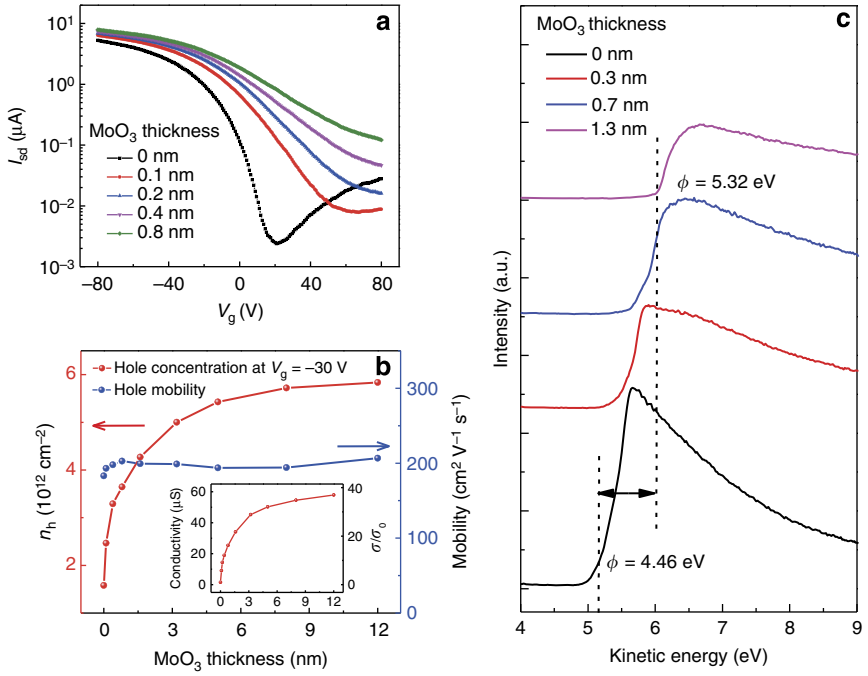

Figure 4 | Hole doping of BP field effect transistor via MoO_3 modification. (**a**) Forward transfer characteristics (V_g from −80 to 80 V) evolution of a separate BP FET measured at V_{sd} = 100 mV with respect to the MoO_3 thickness from 0 to 0.8 nm. (**b**) Hole concentration (n_h) at V_g = −30 V and mobility of BP versus MoO_3 thickness. Inset: BP conductivity at zero gate voltage as a function of MoO_3 thickness. (**c**) UPS spectra evolution at lower kinetic energy region with increasing MoO_3 coverage.

positively shifting with even higher MoO_3 thickness, where the threshold voltage was unreachable for the limited safe gate voltage compliance. It is worth noting that MoO_3 exhibited similar p-type doping effects on BP in bidirectional gate sweeping (Supplementary Fig. 4), suggesting that the existing hysteresis in BP device does not affect the doping effect of MoO_3. Similar to the Cs_2CO_3 doping case, the hole concentration (V_g = −30 V) and mobility was extracted and plotted with respect to MoO_3 thickness in Fig. 4b. After depositing 12 nm MoO_3, the hole concentration of BP at −30 V V_g was increased from 1.6×10^{12} to 5.8×10^{12} cm^{-2}; while the hole mobility almost remained unchanged at ~200 cm^2 V^{-1} s^{-1} even at the high doping level covered by over 10 nm MoO_3. Such retained hole mobility reveals that the hole transport in MoO_3-doped BP was dominated by phonon scattering, and the charge–charge scattering can be ignored in spite of the strongly enhanced hole concentration after doping. After 12 nm MoO_3 decoration, the conductivity of BP FET was largely enhanced from 1.6 to 57.9 μS (inset of Fig. 4b). Four-terminal characterizations on MoO_3-modified BP devices (Supplementary Fig. 5 and Supplementary Table 2) further exhibit much lower contact resistance compared with the channel resistance during MoO_3 deposition.

Similarly, *in situ* UPS/XPS measurements on MoO_3 covered bulk BP were also conducted to examine the underlying interfacial charge transfer mechanism between MoO_3 and BP. As exhibited in Fig. 4c, the UPS spectra of bulk BP gradually evolved towards the higher kinetic energy region with increasing MoO_3 thickness, suggesting that the strong work function increase from 4.46 to 5.32 eV after the deposition of 1.3 nm MoO_3. Owing to the high work function of MoO_3, significant electron transfer from BP to MoO_3 occurred at the MoO_3/BP interface. Furthermore, the obvious upward bend banding was observed in P $2p_{3/2}$ core level XPS spectra with MoO_3 deposition, as shown in Supplementary Fig. 6, indicating the increase of hole concentration in MoO_3-doped BP.

Photodection behaviour of chemically doped BP devices. Arising from a predicted direct bandgap for all number of layers, BP has been used for ultrafast and wide spectrum response photodetectors[29]. In this work, we also evaluated the photodetection properties of BP FETs doped by MoO_3 and Cs_2CO_3 layers. The *in situ* photoresponse measurements were performed by the illumination of a 405-nm laser with the light power of 40 mW (spot diameter 2 mm) exactly after the deposition of surface doping layers in high vacuum chamber. Figure 5a,b shows the time-dependent photoresponse characteristics of BP photodetector with the gradually increased MoO_3 and Cs_2CO_3 thickness, respectively, at V_{sd} = 3 V and V_g = 0 V. The apparent photocurrent enhancement was both identified with increasing MoO_3 and Cs_2CO_3 thickness. After 8.0 nm deposition, the excited photocurrent was largely increased by 3–4 times for both MoO_3 and Cs_2CO_3 cases. Furthermore, the doping process did not severely degrade the response time of BP photodetector, as illustrated in Supplementary Figs 7 and 8, where the rising and decaying time nearly remained at several milliseconds level with increased dopant coverage.

The photoresponsivity (R) and external quantum efficiency (EQE), as two critical parameters of photodetector performance, were calculated and plotted as a function of dopant thickness in Fig. 5c,d. R is defined as the photocurrent generated by per unit power of incident light on the effective area of a photodetector; while EQE is the number of carriers circulating a photodetector per absorbed photon and per unit time[43];

$$R = I_{ph}/(PS) \quad (3)$$

$$\mathrm{EQE} = hcR/(e\lambda) \quad (4)$$

where I_{ph} is the photocurrent induced by incident light, S is the effective area under illumination, P is the light intensity and λ is the wavelength of incident light, and h, c and e represent the Plank constant, velocity of light and the charge of electron,

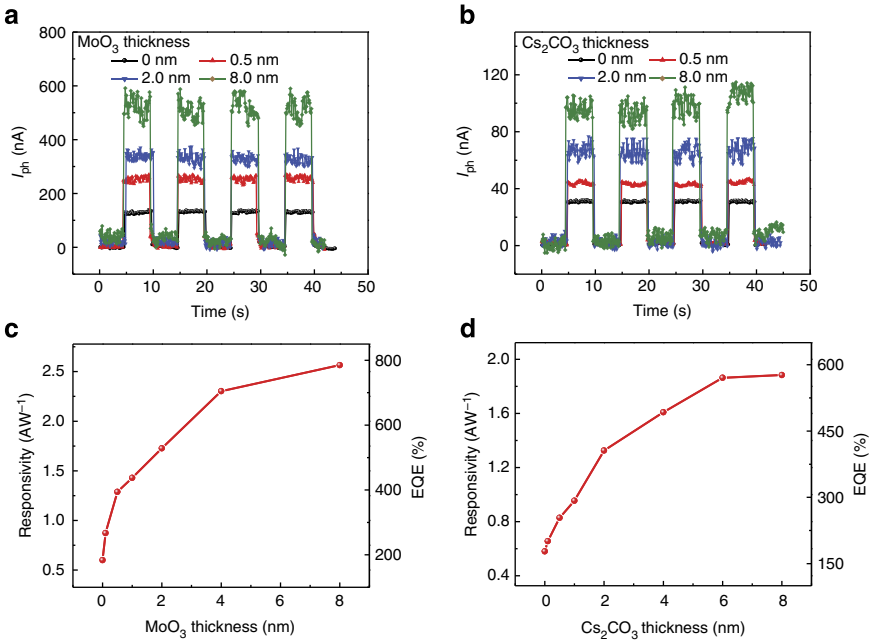

Figure 5 | Time-dependent photoresponse for surface transfer-doped BP photodetectors. Time dependence of photocurrent measured at $V_{sd} = 3$ V upon the illumination of a 405-nm laser source with the power of 40 mW (spot diameter 2 mm) with the *in situ* deposition of (**a**) MoO_3 and (**b**) Cs_2CO_3. Calculated photoresponsivity and EQE as a function of (**c**) MoO_3 and (**d**) Cs_2CO_3 thickness.

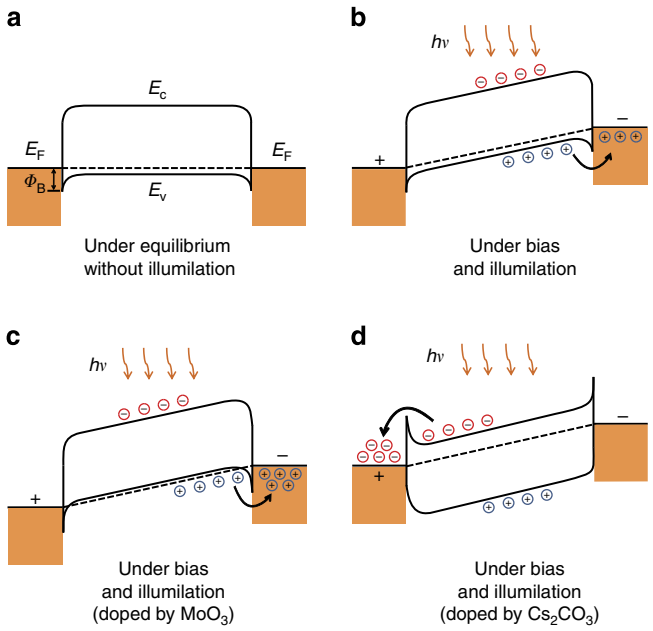

Figure 6 | Qualitative energy band diagrams of BP device through surface transfer doping. Energy band structures between metal contacts and BP (**a**) without and (**b**) with source-drain bias for pristine BP. Energy level alignment with source-drain bias after (**c**) MoO_3 and (**d**) Cs_2CO_3 doping. E_F is the Fermi level energy. Φ_B is the Schottky barrier height. E_C and E_V represent the minimum energy of conduction band and the maximum energy of valance band, respectively. The Schottky barrier formed at metal/BP interface was compressed for both hole and electron doped BP device, facilitating the tunnelling transport of photon excited charge carriers. All the experiments were replicated at least 10 times on separate devices.

respectively. After depositing 8.0 nm doping layers, the responsivity of MoO_3-decorated BP photodetector increased from 0.6 to 2.56 AW^{-1}; while Cs_2CO_3 modification improved the responsivity from 0.58 to 1.88 AW^{-1}. This surface transfer doping enhanced responsivity is much higher than the previously reported BP photodetector[29], even higher than some reported TMDs-based photodetectors, such as MoS_2 (refs 14,44) and WS_2 (ref. 45). Moreover, the MoO_3 and Cs_2CO_3 decoration improved the corresponding EQE from 183% to 784% and from 178% to 576%, respectively, demonstrating an excellent performance enhancement for surface-functionalized BP photodetectors.

The mechanism of the surface doping enhanced photoresponse for BP photodetector is proposed by the modulation of Schottky junction formed at the metal contacts/BP interface, as shown in Fig. 6. Before the application of source-drain bias, the energy level alignment between metal electrodes and BP reached the equilibrium once the physical contacts were established, indicating a non-negligible Schottky barrier between metal contact and BP flake. Upon the illumination of BP device with a source-drain bias, the photo-generated charge carriers in BP channel could undergo a thermal-assisted tunnelling process passing through the Schottky barrier to metal electrode, which contributes to the increase of channel current (Fig. 6b). After the effective hole doping on BP channel by MoO_3, as shown in Fig. 6c, the Fermi level was dragged downwards to the valence band of BP, which compress the Schottky barrier region, and thus reduce the effective barrier height as well as the contact resistance. This significantly facilitates the electrical transport of photo-induced holes, thereby leading to the apparent photocurrent enhancement. Similarly, the electron doping of Cs_2CO_3 pulled the Fermi level towards the BP conduction band, which narrows the Schottky barrier and lowers the contact resistance for electron transport in BP channel. Therefore, the photo-induced electrons could penetrate the barrier more easily, producing the enhanced photoresponse for Cs_2CO_3-modified devices.

Discussion

In this article, we demonstrate effective surface transfer electron and hole doping on few-layer BP FET devices through *in situ* surface functionalization with Cs_2CO_3 and MoO_3 overlayers,

respectively. The electron mobility of BP FETs is found to be significantly enhanced to $\sim 27\,cm^2\,V^{-1}\,s^{-1}$ after 10 nm Cs_2CO_3 modification, giving rise to a highly improved electron transport in the ambipolar characteristics of BP. In contrast, MoO_3 exhibits giant hole-doping effects on BP devices accompanied by the nearly maintained hole mobility of $\sim 200\,cm^2\,V^{-1}\,s^{-1}$. The photodetecting behaviours of surface-doped BP devices are also carefully probed. The responsivity of BP photodetectors is largely enhanced to 2.56 and $1.88\,AW^{-1}$ without degrading response speed after 8.0 nm MoO_3 and Cs_2CO_3 doping, respectively. Our results promise a simple method to either electron or hole dope BP, and thus effectively tailor the ambipolar characteristics of BP FETs to realize the high-performance BP-based complementary logic circuit as well as other functional electronic and optoelectronic devices.

Methods

Sample preparation and device fabrication. Few-layer BP flakes were mechanically exfoliated from bulk BP crystals (Smart Elements) using a scotch tape and transferred onto degenerately p-type-doped silicon wafers coated with 300 nm SiO_2. Exactly after locating the exfoliated BP flake by using high-resolution microscope (Nikon Eclipse LV100D), photoresist PMMA was immediately spin coated onto the sample to protect the flake from being degraded in the air ambient. The source and drain electrodes were precisely patterned on the flake using the conventional e-beam lithography technique, followed by thermal evaporation of Ti (5 nm) and Au (80 nm) as the metal contacts. After liftoff, the as-made devices were wire bonded onto a leaded chip carrier (LCC) and loaded in a custom-designed high vacuum system ($\sim 10^{-8}$ mbar) for *in situ* electrical measurements.

***In situ* device characterization.** FET characterizations were carried out using an Agilent 2912A source measure unit at room temperature. Cs_2CO_3 and MoO_3 were separately evaporated *in situ* from a Knudsen cell onto the devices in high vacuum chamber. The nominal thickness of Cs_2CO_3 and MoO_3 layers was calibrated by a quartz crystal microbalance exactly located in front of the sample stage. *In situ* photoresponse measurements were also conducted right after the deposition of doping layers in the high vacuum chamber. The sample was illuminated by a 405-nm laser with power of 40 mW (spot diameter 2.0 mm).

***In situ* UPS and XPS characterization.** *In situ* UPS and XPS measurements on both MoO_3- and Cs_2CO_3-coated bulk BP were carried out in a home-made ultrahigh vacuum chamber (10^{-10} mbar) with He I (21.2 eV) and Mg Kα (1,253.6 eV) as excitation sources, respectively. By applying a sample bias of -5 V, the sample work function was determined by the secondary electron cutoff at the low kinetic energy region. The nominal thickness of *in situ* deposited Cs_2CO_3 and MoO_3 layers was estimated by the attenuation of P $2p_{3/2}$ peak and further calibrated by quartz crystal microbalance.

References

1. Helveg, S. *et al.* Atomic-scale structure of single-layer MoS_2 nanoclusters. *Phys. Rev. Lett.* **84,** 951–954 (2000).
2. Liu, H., Neal, A. T. & Ye, P. D. Channel length scaling of MoS_2 MOSFETs. *ACS Nano* **6,** 8563–8569 (2012).
3. Leitao, L., Bala Kumar, S., Yijian, O. & Guo, J. Performance limits of monolayer transition metal dichalcogenide transistors. *IEEE Trans. Electron Dev.* **58,** 3042–3047 (2011).
4. Pang, S., Hernandez, Y., Feng, X. & Müllen, K. Graphene as transparent electrode material for organic electronics. *Adv. Mater.* **23,** 2779–2795 (2011).
5. Wang, Y., Chen, X., Zhong, Y., Zhu, F. & Loh, K. P. Large area, continuous, few-layered graphene as anodes in organic photovoltaic devices. *Appl. Phys. Lett.* **95,** 063302 (2009).
6. Geim, A. K. & Novoselov, K. S. The rise of graphene. *Nat. Mater.* **6,** 183–191 (2007).
7. Bolotin, K. I. *et al.* Ultrahigh electron mobility in suspended graphene. *Solid State Commun.* **146,** 351–355 (2008).
8. Novoselov, K. S. *et al.* Two-dimensional gas of massless Dirac fermions in graphene. *Nature* **438,** 197–200 (2005).
9. Zhang, Y., Tan, Y.-W., Stormer, H. L. & Kim, P. Experimental observation of the quantum Hall effect and Berry's phase in graphene. *Nature* **438,** 201–204 (2005).
10. Castro Neto, A. H., Guinea, F., Peres, N. M. R., Novoselov, K. S. & Geim, A. K. The electronic properties of graphene. *Rev. Mod. Phys.* **81,** 109–162 (2009).
11. Schwierz, F. Graphene transistors. *Nat. Nano* **5,** 487–496 (2010).
12. Radisavljevic, B., Radenovic, A., Brivio, J., Giacometti, V. & Kis, A. Single-layer MoS_2 transistors. *Nat. Nano* **6,** 147–150 (2011).
13. Fang, H. *et al.* High-performance single layered WSe_2 p-FETs with chemically doped contacts. *Nano Lett.* **12,** 3788–3792 (2012).
14. Yin, Z. *et al.* Single-layer MoS_2 phototransistors. *ACS Nano* **6,** 74–80 (2011).
15. Popov, I., Seifert, G. & Tománek, D. Designing electrical contacts to MoS_2 monolayers: a computational study. *Phys. Rev. Lett.* **108,** 156802 (2012).
16. Das, S., Chen, H.-Y., Penumatcha, A. V. & Appenzeller, J. High performance multilayer MoS_2 transistors with scandium contacts. *Nano Lett.* **13,** 100–105 (2012).
17. Wang, H. *et al.* Integrated circuits based on bilayer MoS_2 transistors. *Nano Lett.* **12,** 4674–4680 (2012).
18. Radisavljevic, B., Whitwick, M. B. & Kis, A. Integrated circuits and logic operations based on single-Layer MoS_2. *ACS Nano* **5,** 9934–9938 (2011).
19. Ross, J. S. *et al.* Electrically tunable excitonic light-emitting diodes based on monolayer WSe_2 p-n junctions. *Nat. Nano* **9,** 268–272 (2014).
20. Pospischil, A., Furchi, M. M. & Mueller, T. Solar-energy conversion and light emission in an atomic monolayer p-n diode. *Nat. Nano* **9,** 257–261 (2014).
21. Baugher, B. W. H., Churchill, H. O. H., Yang, Y. & Jarillo-Herrero, P. Optoelectronic devices based on electrically tunable p-n diodes in a monolayer dichalcogenide. *Nat. Nano* **9,** 262–267 (2014).
22. Liu, W. *et al.* Role of metal contacts in designing high-performance monolayer n-type WSe_2 field effect transistors. *Nano Lett.* **13,** 1983–1990 (2013).
23. Li, L. *et al.* Black phosphorus field-effect transistors. *Nat. Nano* **9,** 372–377 (2014).
24. Xia, F., Wang, H. & Jia, Y. Rediscovering black phosphorus as an anisotropic layered material for optoelectronics and electronics. *Nat. Commun.* **5,** 4458 (2014).
25. Du, Y., Ouyang, C., Shi, S. & Lei, M. Ab initio studies on atomic and electronic structures of black phosphorus. *J. Appl. Phys.* **107,** 093718 (2014).
26. Prytz, Ø. & Flage-Larsen, E. The influence of exact exchange corrections in van der Waals layered narrow bandgap black phosphorus. *J. Phys. Condens. Matter* **22,** 015502 (2010).
27. Narita, S. *et al.* Electrical and optical properties of black phosphorus single crystals. *Physica* **117B–118B,** 422–424 (1983).
28. Maruyama, Y., Suzuki, S., Kobayashi, K. & Tanuma, S. Synthesis and some properties of black phosphorus single crystals. *Physica* **105,** 99–102 (1981).
29. Buscema, M. *et al.* Fast and broadband photoresponse of few-layer black phosphorus field-effect transistors. *Nano Lett.* **14,** 3347–3352 (2014).
30. Koenig, S. P., Doganov, R. A., Schmidt, H., Castro Neto, A. H. & Özyilmaz, B. Electric field effect in ultrathin black phosphorus. *Appl. Phys. Lett.* **104,** 103106 (2014).
31. Castellanos-Gomez, A. *et al.* Isolation and characterization of few-layer black phosphorus. *2D Mater.* **1,** 025001 (2014).
32. Han, C. *et al.* Improving chemical vapor deposition graphene conductivity using molybdenum trioxide: an in-situ field effect transistor study. *Appl. Phys. Lett.* **103,** 263117 (2013).
33. Lin, J. D. *et al.* Electron-doping-enhanced trion formation in monolayer molybdenum disulfide functionalized with cesium carbonate. *ACS Nano* **8,** 5323–5329 (2014).
34. Kröger, M. *et al.* P-type doping of organic wide band gap materials by transition metal oxides: a case-study on molybdenum trioxide. *Org. Electron.* **10,** 932–938 (2009).
35. Zhou, X. *et al.* Enhanced hole injection into amorphous hole-transport layers of organic light-emitting diodes using controlled p-type doping. *Adv. Funct. Mater.* **11,** 310–314 (2001).
36. Fang, H. *et al.* Degenerate n-doping of few-layer transition metal dichalcogenides by potassium. *Nano Lett.* **13,** 1991–1995 (2013).
37. Buscema, M., Groenendijk, D. J., Steele, G. A., van der Zant, H. S. J. & Castellanos-Gomez, A. Photovoltaic effect in few-layer black phosphorus PN junctions defined by local electrostatic gating. *Nat. Commun.* **5,** 4651–4655 (2014).
38. Junwei, M. *et al.* Highly power efficient organic light-emitting diodes based on Cs_2CO_3 n-doped and MoO_3 p-doped carrier transport layers. *Semicond. Sci. Technol.* **24,** 035009 (2009).
39. Sugai, S. & Shirotani, I. Raman and infrared reflection spectroscopy in black phosphorus. *Solid State Commun.* **53,** 753–755 (1985).
40. Cai, Y. *et al.* Mechanism of Cs_2CO_3 as an n-type dopant in organic electron-transport film. *Appl. Phys. Lett.* **98,** 113304 (2011).
41. Barbot, A., Lucas, B., Di Bin, C., Ratier, B. & Aldissi, M. Optimized inverted polymer solar cells incorporating Cs_2CO_3-doped C_{60} as electron transport layer. *Appl. Phys. Lett.* **102,** 193305 (2013).
42. Chen, Z. *et al.* Surface transfer hole doping of epitaxial graphene using MoO_3 thin film. *Appl. Phys. Lett.* **96,** 213104 (2010).
43. Li, L. *et al.* Ultrahigh-performance solar-blind photodetectors based on individual single-crystalline $In_2Ge_2O_7$ nanobelts. *Adv. Mater.* **22,** 5145–5149 (2010).
44. Choi, W. *et al.* High-detectivity multilayer MoS_2 phototransistors with spectral response from ultraviolet to infrared. *Adv. Mater.* **24,** 5832–5836 (2012).
45. Perea-López, N. *et al.* Photosensor device based on few-layered WS_2 films. *Adv. Funct. Mater.* **23,** 5511–5517 (2013).

Acknowledgements

We acknowledge the technical support from Graphene Research Centre at National University of Singapore (NUS) for the device fabrication, and financial support from Singapore MOE Grant R143-000-559-112 and National Key Basic Research Program of China (2015CB856505).

Author contributions

D.X., C.H. and J.W. contributed equally to this paper. W.C. supervised the experiments. D.X., C.H., J.W. and S. Z. performed the experiments. C.H., D.X. and W.C. wrote the main manuscript. D.X., C.H. and J.W. prepared Figs1–6. D.X. and C.H. prepared Supplementary Figs 1–8. All authors reviewed the manuscript.

Additional information

Supplementary Information accompanies this paper at http://www.nature.com/naturecommunications

Competing financial interests: The authors declare no competing financial interests.

Reprints and permission information is available online at http://npg.nature.com/reprintsandpermissions/

How to cite this article: Xiang, D. *et al.* Surface transfer doping induced effective modulation on ambipolar characteristics of few-layer black phosphorus. *Nat. Commun.* 6:6485 doi: 10.1038/ncomms7485 (2015).